Research Square

Preprints are preliminary reports that have not undergone peer review.
They should not be considered conclusive, used to inform clinical practice,
or referenced by the media as validated information.

Transcriptomic Reprogramming of Peripheral Blood Mononuclear Cells Induced by Lung Cancer

Ratakorn Srisuttee
King Mongkut's Institute of Technology Ladkrabang
Suthipong Chujan
Chulabhorn Research Institute
Apiwat Mutirangura
Chulalongkorn University
Pisak Ongsirimonkol
Burapha University
Nakarin Kitkumthorn
nakarinkit@gmail.com

Burapha University

Article

Keywords: Lung cancer, Peripheral blood mononuclear cells, RNA sequencing, Tumor-immune interaction, Transcriptome

Posted Date: October 12th, 2026

DOI: https://doi.org/10.21203/rs.3.rs-11050339/v1

License: This work is licensed under a Creative Commons Attribution 4.0 International License.
Read Full License

Additional Declarations: No competing interests reported.

Abstract

Paracrine signaling from lung cancer cells can profoundly influence immune function, but its systemic impact on peripheral blood mononuclear cells (PBMCs) is poorly understood. This study characterizes transcriptomic changes in PBMCs exposed to lung cancer secretions to identify immune-associated clinical signatures.

Methods: PBMCs from healthy donors were co-cultured with A549 or H292 lung cancer cell lines for 4 hours, followed by RNA sequencing. Differentially expressed genes (DEGs) were analyzed using GO/KEGG enrichment, integrated with public microarray datasets, and validated clinically via TIMER2.0.

Results: Co-culture induced extensive transcriptional reprogramming, yielding 296 differentially expressed genes (DEGs) in the A549 model and 508 in the H292 model. Statistical filtering identified a conserved signature of 21 commonly altered genes (including *ANKRD37*, *BUB3*, *IL6*, *CSF3*, and *INHBA*). *ANKRD37* and *BUB3* were consistently validated across independent clinical datasets. Enrichment analysis revealed shared activation of NOD-like receptor signaling, alongside line-specific metabolic and biosynthetic pathway alterations. Furthermore, *BUB3* expression positively correlated with activated $CD4^+$ T-cell infiltration, while *ANKRD37* negatively associated with $CD8^+$ T cells.

Conclusions: Lung cancer secretions drive systemic immune reprogramming in PBMCs. This reflects a systemic-to-local tumor–immune axis and highlights *ANKRD37* and *BUB3* as candidate circulating biomarkers.

Introduction

Lung cancer remains the leading cause of cancer-related death worldwide, with approximately 1.8 million deaths each year, accounting for about 18% of all cancer deaths[1]. Although treatment strategies have improved, the overall 5-year survival rate is still around 22%, indicating the need to better understand the molecular mechanisms involved in lung cancer development[2]. Increasing evidence has shown that lung cancer cells can release various soluble factors that modulate the tumor microenvironment and promote tumor growth, invasion, and metastasis. These secreted factors include cytokines, chemokines, growth factors, and extracellular vesicles, which can affect nearby stromal cells, endothelial cells, and immune cells through paracrine signaling[3, 4].

Peripheral blood mononuclear cells (PBMCs), including lymphocytes and monocytes, play important roles in systemic anti-tumor immune responses[5, 6]. Previous studies demonstrated that secretory products from different cancers can alter the epigenetic and transcriptional profiles of surrounding cells, potentially changing their functions[7–9]. In breast cancer, tumor secretions were reported to induce epigenetic changes in nearby stromal cells[10]. However, the effects of lung cancer cell secretions on circulating PBMCs, which serve as an important first-line immune defense against tumors, are still not well understood.

Previous reports showed that cancer cell secretions can remodel the epigenomic and transcriptomic landscapes of surrounding cells[11, 12]. Based on these findings, we hypothesized that molecules released by lung cancer cells may influence the transcriptome of PBMCs, key mediators of anti-tumor immunity. To investigate this hypothesis, PBMCs from healthy donors were co-cultured with lung cancer cell lines, and gene expression profiles between co-cultured and uncultured control PBMCs were compared using RNA sequencing. In addition, transcriptomic profiling, bioinformatic analysis, and comparison with patient datasets were performed to identify molecular mechanisms involved in lung cancer–immune cell interactions, which may contribute to cancer progression and future therapeutic approaches.

Results

Identification of Differentially Expressed Genes in PBMCs Following Co-culture with Lung Cancer Cells

The overall study design was shown in Fig. 1. To investigate the effects of lung cancer-derived factors on immune-related gene expression, PBMCs were co-cultured with A549 and H292 lung cancer cell lines, and RNA-seq analysis was performed. A large number of transcriptional changes were observed in both co-culture conditions, with nearly 16,000 genes showing altered expression patterns in each group (Fig. 2A). After applying the statistical cutoff ($p < 0.05$), 170 up-regulated genes and 126 down-regulated genes were identified in PBMCs co-cultured with A549 cells. In the H292 co-culture model, 302 genes were significantly up-regulated, whereas 206 genes were down-regulated. Venn diagram analysis demonstrated that 21 genes were commonly altered in PBMCs exposed to both lung cancer cell lines (Fig. 2B-C). Among these, 12 genes were consistently up-regulated, including *ANKRD37*, *BUB3*, *CSF3*, *IL6*, and *INHBA*. Interestingly, *CSF3* and *IL6* showed relatively high fold changes compared with other genes, with expression increases reaching around 8-fold. On the other hand, 9 genes were commonly down-regulated, such as *CAMSAP2*, *G6PD*, and *TGFBI*. These findings suggest that lung cancer cells may induce similar transcriptional responses in PBMCs regardless of the cell line used in the co-culture system. The common gene set identified in this study may reflect conserved immune-related responses associated with lung cancer-derived secreted factors and could be useful for further studies on biomarkers or tumor–immune interactions.

Functional Enrichment Analysis of DEGs Reveals Cell-Line Specific and Conserved Immune Responses

GO and KEGG enrichment analyses were performed to investigate the biological functions and signaling pathways associated with the differentially expressed genes (DEGs) identified in PBMCs after co-culture with lung cancer cells (Fig. 3). The results showed that both A549 and H292 co-culture models shared several immune-related responses, especially pathways associated with NOD-like receptor signaling and cytokine-related activity. However, some functional differences between the two cell lines were also observed. In the H292 co-culture group, GO analysis demonstrated significant enrichment of genes

involved in NOD2 signaling and cytokine activity, with enrichment scores of approximately 4.5 and 3.5, respectively (Fig. 3A). KEGG pathway analysis further identified ribosome biogenesis as the most enriched pathway in the H292 group, showing a fold enrichment greater than 6.0 and high statistical significance (Fig. 3B). Pathway analysis also demonstrated increased expression of several genes associated with ribosomal RNA processing, particularly components involved in the 90S pre-ribosome and small subunit processes.

For the A549 co-culture condition, enrichment analysis suggested changes related to cellular metabolism. Although GO analysis showed common pathways related to NOD2 signaling and carbohydrate biosynthesis (Fig. 3C), KEGG analysis identified the pentose phosphate pathway as the most significantly enriched pathway, with a fold enrichment greater than 12.5 (Fig. 3D). Biosynthesis of amino acids and TNF signaling pathways were also enriched. In addition, pathway mapping revealed increased expression of important metabolic enzymes, including glucose-6-phosphate dehydrogenase and 6-phosphogluconate dehydrogenase, which are involved in NADPH production and oxidative balance. Taken together, these findings indicate that secreted factors from different lung cancer cell lines may induce distinct responses in PBMCs. H292 cells appeared to mainly affect ribosome-related processes, whereas A549 cells were more associated with metabolic pathway alterations, particularly the pentose phosphate pathway.

Validation of Paracrine-Responsive Genes Using Clinical Lung Cancer PBMC Datasets

To investigate whether the gene expression changes observed in our co-culture models were also present in lung cancer patients, RNA-seq results were compared with four independent PBMC transcriptomic datasets obtained from clinical lung cancer samples (Fig. 4). Fisher's exact test demonstrated significant overlap between genes identified in the co-culture models and those detected in patient datasets for both up-regulated and down-regulated genes. For the up-regulated gene sets, 29 overlapping genes were identified between the A549 co-culture model and clinical datasets, with an odds ratio (OR) of 2.47 and a p-value of 0.00000677. In the H292 co-culture model, 37 overlapping genes were observed, showing an OR of 1.62 and a p-value of 0.00657 (Fig. 4A). Similar findings were also detected in the down-regulated gene groups. A total of 24 shared genes were identified between A549-treated PBMCs and patient datasets (OR = 2.00, p = 0.00281), while the H292 model showed 35 overlapping genes (OR = 1.57, p = 0.0172) (Fig. 4B). To identify genes that were consistently altered in both experimental and clinical conditions, overlapping analysis was performed using the validated up-regulated genes from both co-culture models (Fig. 4C). Among the identified genes, *ANKRD37* and *BUB3* were consistently up-regulated across both lung cancer cell lines and all patient datasets. In contrast, no common genes were identified among the down-regulated groups. These results suggest that *ANKRD37* and *BUB3* may represent potential molecular markers associated with lung cancer-related paracrine effects on PBMCs.

Association Between ANKRD37 and BUB3 Expression and Immune Cell Infiltration in Lung Cancer

To explore the potential relationship between *ANKRD37* and *BUB3* expression and the tumor immune microenvironment, correlation analysis was performed using the TIMER2.0 database in Lung Adenocarcinoma (LUAD) and Lung Squamous Cell Carcinoma (LUSC). As shown in Fig. 5A, the two genes demonstrated different patterns of association with immune cell infiltration. *BUB3* expression was generally positively correlated with immune cell populations, particularly CD8 + T cells and CD4 + T cells, across several analytical algorithms. In contrast, *ANKRD37* expression showed mainly negative correlations with CD8 + and CD4 + T-cell infiltration, especially in LUAD samples. Different levels of association with B cells and monocytes were also observed, although *BUB3* tended to show stronger positive correlations with lymphocyte-related populations. The detailed correlation plots presented in Fig. 5B further supported these findings. In LUSC, *ANKRD37* expression showed a significant negative correlation with CD8 + T-cell infiltration (Spearman's rho = − 0.162, $p = 3.93 \times 10^{-4}$). On the other hand, *BUB3* expression demonstrated positive correlations with activated CD4 + T cells in LUAD (Rho = 0.37, $p = 2.11 \times 10^{-17}$) and with CD8 + T cells in LUSC (Rho = 0.173, $p = 1.44 \times 10^{-4}$). Interestingly, *BUB3* expression was negatively associated with memory B cells in LUAD (Rho = − 0.228, $p = 3.27 \times 10^{-7}$). Overall, these results indicate that *ANKRD37* and *BUB3* may have different relationships with immune cell infiltration in lung cancer. While both genes were identified as paracrine-responsive genes in PBMCs, their opposite correlation patterns with tumor-infiltrating lymphocytes suggest potentially distinct roles in the regulation of the tumor immune microenvironment.

Discussion

This study demonstrates that lung cancer secretome drives systemic immune reprogramming, as evidenced by distinct transcriptomic and metabolic alterations in PBMCs. A core set of 21 paracrine-responsive genes, including *ANKRD37* and *BUB3*, was consistently identified and validated across clinical datasets. While both A549 and H292 models activated inflammatory pathways such as NOD-like receptor signaling and cytokine production, they induced divergent programs, with H292 enhancing protein synthesis and ribosome biogenesis, and A549 promoting a shift toward the pentose phosphate pathway. These findings highlight that tumor-derived factors shape specific systemic immune states in a context-dependent manner.

The 4-hour co-culture of PBMCs with A549 and H292 cells induced a strong transcriptional shift, affecting nearly 16,000 genes (~ 8,000 up- and ~ 8,000 down-regulated). This extent of change is much higher than the 1,334–1,450 DEGs reported in PBMCs from HCC patients[13, 14] and the 367 DEGs observed in HCC cell co-culture models[15], and is more comparable to the global dysregulation reported in lung cancer or TB studies (4,438–4,865 DEGs)[16]. Such rapid and large-scale reprogramming may reflect an acute paracrine response driven by cancer-derived secretomes and exosomes[17, 18]. Notably, strong up-regulation of *IL6*, *CSF3*, and *INHBA* (up to ~ 8-fold), together with stress-related genes *ANKRD37* and *TXNIP*, suggests marked non-homeostatic stimulation and metabolic adaptation[13, 14, 19].

In contrast, down-regulation of *G6PD* and *TGFBI* differs from patterns typically reported in chronic HCC-related immune changes[13, 14]. This bidirectional gene response indicates early systemic stress and immune reprogramming and highlights these conserved genes as potential systemic biomarkers, similar to cancer-induced gene signatures observed in other malignancy models[15].

Functional enrichment analysis suggests that lung cancer secretome rapidly induces a coordinated pattern of innate immune sensing and metabolic reprogramming in PBMCs. The shared activation of NOD-like receptor (NLR) signaling and cytokine-related pathways in both models is consistent with the concept that tumor-derived damage-associated molecular patterns (DAMPs) can activate cytosolic NLRs, leading to systemic sterile inflammation through RIP2 and NF-κB signaling pathways[20–22]. In a cell line–specific manner, A549-induced DEGs were mainly enriched in the pentose phosphate pathway (PPP) and TNF signaling, indicating metabolic rerouting toward NADPH production and antioxidant defense, which is commonly observed in activated immune cells under oxidative stress[23–25]. In contrast, H292 co-culture showed stronger enrichment in ribosome biogenesis and NOD2 signaling, suggesting a response more focused on protein synthesis capacity and cytokine responsiveness[26, 27]. These differences may be related to variations in DAMP composition between adenocarcinoma (A549) and mucoepidermoid (H292) secretomes[25, 28, 29]. The enrichment of NLR signaling, PPP, and ribosomal pathways indicates that PBMCs are driven into a metabolically demanding and highly activated state, which may support inflammatory functions but also increase susceptibility to metabolic stress and exhaustion.

Integrative validation using independent lung cancer PBMC cohorts supports that the *in vitro* paracrine-responsive signature reflects systemic immune alterations in patients. The overlap between our co-culture models and clinical datasets was significant (A549: 29 genes, OR = 2.47, $p < 0.0001$; H292: 37 genes, OR = 1.62, $p = 0.006$), and these values are within the range reported for established blood-based lung cancer classifiers (OR/HR 2–4, AUC 0.69–0.91)[30, 31]. Within this shared signature, *ANKRD37* and *BUB3* were consistently upregulated across all datasets. *ANKRD37*, a hypoxia-inducible HIF-1α target associated with poor prognosis, may reflect systemic cellular responses to tumor-related hypoxic signaling[32], whereas *BUB3* is linked to cell-cycle regulation and proliferative stress in aggressive disease[33, 34]. The consistent detection of these genes across adenocarcinoma, mucoepidermoid, and patient-derived cohorts suggests a common tumor-induced systemic stress response rather than cell line-specific effects. Therefore, *ANKRD37* and *BUB3* may serve as potential biomarkers for monitoring tumor–immune interactions in peripheral blood.

Analysis using TIMER2.0 shows that *BUB3* and *ANKRD37* are associated with opposite patterns of T-cell infiltration in lung cancer tissues. *BUB3* expression was positively correlated with CD8 + and CD4 + T cells, including a moderate correlation with activated CD4 + T cells (Rho ≈ 0.37, $p < 0.0001$), which is similar to patterns reported in “hot” tumor microenvironments associated with better immune checkpoint inhibitor (ICI) response[35–37]. This pattern is also consistent with non-canonical cell-cycle-related genes that correlate with cytotoxic T lymphocyte (CTL) infiltration[36, 38]. In contrast, *ANKRD37*

showed a significant negative correlation with CD8 + T-cell infiltration in LUAD (Rho = − 0.162, $p < 0.001$), which is in line with hypoxia- and HIF-related mechanisms linked to immune exclusion and “cold” tumor phenotypes[39, 40]. These observations, together with previous reports in HCC and LUAD where blood-derived signatures reflect intratumoral immune status, suggest a connection between systemic PBMC markers and local immune infiltration patterns[38, 41]. Overall, the results indicate that *BUB3* is associated with a more inflamed, T-cell–rich tumor environment, while *ANKRD37* is linked to hypoxia-associated immune suppression, which may have implications for ICI responsiveness.

Building on this systemic-to-local relationship, *BUB3* appears to be a more promising biomarker candidate with higher translational potential compared with *ANKRD37*. It is consistently upregulated in PBMCs in both A549 and H292 co-culture models and is also present across all clinical datasets, supporting its reproducibility. In LUAD tissues, *BUB3* is significantly overexpressed and associated with poorer survival outcomes (HR = 1.7, $p = 0.00026$), as well as clinical features such as lymph node metastasis, TP53 mutation, and smoking status[42, 43]. These findings are consistent with our integrative analysis and suggest that *BUB3* may reflect both tumor progression and immune activity. In contrast to *ANKRD37*, which is mainly linked to hypoxia-related responses, *BUB3* shows a more direct association with T-cell infiltration and patient prognosis, supporting its relevance in an inflamed tumor microenvironment. This suggests that *BUB3* may be useful for monitoring changes in tumor–immune interactions over time. Therefore, inclusion of *BUB3* in a liquid biopsy panel may improve patient stratification and support clinical decision-making for immunotherapy.

In conclusion, this study provides a comprehensive characterization of systemic immune reprogramming induced by lung cancer-derived paracrine factors. A conserved 21-gene signature was identified in PBMCs, with *ANKRD37* and *BUB3* emerging as high-confidence biomarkers and validated across multiple clinical datasets. Functionally, lung cancer secretomes induced a bifurcated immune response, characterized by shared activation of NOD-like receptor signaling together with distinct programs involving ribosome biogenesis in H292 and the pentose phosphate pathway in A549. Importantly, the systemic expression of these genes mirrors the intratumoral immune landscape, where *BUB3* is associated with T-cell-inflamed tumors, whereas *ANKRD37* correlates with immune exclusion. These findings support a systemic-to-local axis of tumor–immune interaction and suggest that peripheral blood transcripts may serve as non-invasive biomarkers for monitoring immune status and predicting responses to immunotherapy in lung cancer patients.

Methods

Cell culture and maintenance of lung cancer Cell Lines

The lung cancer cell lines, A549 and H292, were purchased from the American Type Culture Collection (ATCC, Manassas, VA, USA) cultured in Dulbecco’s modified Eagle medium (DMEM) (Gibco BRL, USA) supplemented with 10% heat-inactivated fetal calf serum, 1% penicillin (100 U/mL), and streptomycin

(100 µg/mL). The cells were maintained at 37°C in a humidified incubator containing 5% carbon dioxide and 95% air under standard culture conditions.

Isolation and co-culture of PBMCs with lung cancer cell lines

Peripheral blood mononuclear cells (PBMCs) were isolated from heparinized blood samples obtained from three healthy male and three healthy female volunteers. Blood samples were layered onto lymphocyte separation medium at a 1:1 ratio and centrifuged at 2600 rpm for 15 minutes. The PBMC layer, observed as a distinct white ring at the interface, was carefully collected and washed twice with phosphate-buffered saline (PBS). The isolated PBMCs were resuspended in 1 mL of PBS for subsequent co-culture experiments. The co-culture system was established using 24-well Transwell membrane plates (Corning Inc., Corning, NY, USA). A549 and H292 lung cancer cells were seeded separately into 24-well plates containing 200 µL of DMEM per well. Subsequently, 100,000 PBMCs were added to the Transwell membrane inserts with 100 µL of DMEM in the upper chamber. The co-culture systems were incubated at 37°C in a humidified atmosphere containing 5% CO2 and 95% air for 4 hours. After incubation, PBMCs from the membrane inserts were collected for subsequent RNA extraction.

RNA extraction from co-cultured PBMCs

Total RNA extraction from PBMCs was performed using TRIzol LS reagent (Thermo Scientific™, Waltham, MA, USA) following the manufacturer's protocol (Thermo Fisher Scientific, 2016). Briefly, PBMCs were mixed with 1 mL of TRIzol LS reagent and incubated at room temperature for 5 minutes. Subsequently, 200 µL of chloroform was added, followed by an additional 3-minutes incubation at room temperature. The resulting mixture was centrifuged at 8760 RPM and 4°C for 15 minutes, leading to the separation into three distinct phases. The upper aqueous phase, devoid of color, was carefully transferred to a new RNA tube, and alcohol precipitation was conducted. The RNA pellet was then resuspended in 30 µL of diethyl pyrocarbonate-treated water and quantified using a Qubit Fluorometer (Thermo Scientific™, Waltham, MA, USA). To evaluate the RNA's quality before sequencing, the RNA 6000 Nano Assay (Agilent Technologies, Santa Clara, CA, USA) was employed, with a recommended threshold of an RNA integrity number greater than 7. RNA samples with a concentration of at least 1 µg were subsequently utilized for RNA sequencing analysis.

RNA sequencing and analysis

For RNA sequencing library preparation, 200 ng of total RNA was used. Poly-A mRNA was enriched using oligo-dT beads, and complementary DNA (cDNA) was synthesized using random primers. Library preparation was performed using the NEBNext® Ultra™ RNA Library Prep Kit according to the manufacturer’s instructions (Illumina Inc., San Diego, CA, USA; New England Biolabs, 2018). The prepared libraries were ligated with P5 and P7 adapters and amplified by PCR for 11 cycles. The resulting double-stranded cDNA libraries were sequenced on the Illumina HiSeq platform using 150 bp paired-end

reads. All RNA-sequencing data underwent quality control analysis using FastQC, and only reads with Q scores greater than 30 were included. Sequence reads were aligned to the human reference genome (GRCh38.p10) using HISAT2 version 2.1.0 based on the hierarchical indexing method for spliced transcript alignment described by Pertea et al.[12]. Transcript assembly was performed using StringTie version 1.3.3b. Differential gene expression analysis between co-culture and control groups was conducted using DESeq2 version 1.16.1, as recommended in the StringTie workflow[11]. Differentially expressed genes were categorized into up-regulated and down-regulated groups based on fold change and adjusted p-value criteria (Fig. 1). All raw and processed RNA sequencing data generated in this study have been deposited in the Gene Expression Omnibus database under accession number GSE112005.

Bioinformatic analysis

In this study, publicly available gene expression datasets of peripheral blood mononuclear cells (PBMCs) from lung cancer patients and healthy individuals were retrieved from the Gene Expression Omnibus database. The selected datasets included GSE12771-GPL6102, GSE12771-GPL6097, GSE13255-GPL6102, and GSE39345-GPL6104. Data analysis was performed using the CU-DREAM extension program to identify up-regulated candidate genes, down-regulated candidate genes, and genes potentially influenced by paracrine signaling (Fig. 1).

Biological function alteration and enrichment pathway analysis

The differentially expressed genes (DEGs) identified from PBMCs co-cultured with A549 and H292 cells were analyzed using the DAVID database for functional enrichment analysis. Statistical significance was defined as $p < 0.05$. Gene Ontology (GO) analysis was performed to evaluate biological process (BP), cellular component (CC), and molecular function (MF) categories. In addition, pathway enrichment analysis was conducted using the Kyoto Encyclopedia of Genes and Genomes (KEGG) database to identify significantly associated signaling pathways.[44,45]

Immune association analysis

To investigate the association between gene expression and immune response, *ANKRD37* and *BUB3* were analyzed using the Tumor Immune Estimation Resource (TIMER) database. TIMER was used to evaluate the correlation between gene expression and immune cell infiltration in cancer tissues. Statistical significance was assessed using log-rank *p*-values and hazard ratios (HRs) with 95% confidence intervals (CIs). A positive correlation was defined as $p < 0.05$ with Spearman's $\rho > 0$, whereas a negative correlation was defined as $p < 0.05$ with Spearman's $\rho < 0.05$.

Statistical analysis

Statistical analyses were performed using SPSS Statistics (SPSS Inc., Chicago, IL, USA). Student's t-test and chi-square test were used to evaluate significant differences in gene expression and the distribution of up-regulated and down-regulated genes identified by the CU-DREAM program, respectively. Data are

presented as mean ± standard deviation (SD), and all adjusted *p*-values were two-sided. A *p*-value of less than 0.05 was considered statistically significant.

Declarations

Ethics Approval and Consent to Participate: This study was approved by the Ethics Committee of the Institutional Review Board of the Faculty of Medicine, Chulalongkorn University (COA No. 256/2016, IRB No. 034/59) and followed the principles of the Declaration of Helsinki. Before blood collection, all participants received clear information about the study goals, the blood sampling procedure, and potential risks. All participants gave written informed consent before taking part in the study**.**

Author Contributions: R.S. and N.K. conceived the study, designed the methodology, curated the data, and drafted the manuscript. R.S., S.C., and N.K. performed the experiments, analyzed the data, and prepared the figures. A.M. and N.K. supervised the research and provided resources. R.S. and AM acquired funding and administered the project. R.S., P.O., and N.K. critically revised the manuscript. All authors reviewed and approved the final manuscript.

Acknowledgement: Not applicable.

Funding: This study was supported by Chulalongkorn University and King Mongkut's Institute of Technology Ladkrabang, Bangkok, Thailand.

Disclosure: All the authors have read and approved the final version of the manuscript.

Conflicts of interest: The authors declare no conflict of interest.

Data Availability Statement: The datasets generated and/or analyzed during the current study are available in the Gene Expression Omnibus (GEO) repository, accession number GSE112005.

References

1. Zhang N, Hao J, Cai Y & Wang M. Research advances of secretory proteins in malignant tumors. *Chinese Journal of Cancer Research*. 33(1), 115 (2021).
2. Wu YY et al. SCUBE3 is an endogenous TGF-beta receptor ligand and regulates the epithelial-mesenchymal transition in lung cancer. *Oncogene*. 30(34), 3682. https://doi.org/10.1038/onc.2011.85 (2011).
3. Wang C et al. Secreted pyruvate kinase M2 promotes lung cancer metastasis through activating the integrin Beta1/FAK signaling pathway. *Cell Rep*. 30(6), 1780 e1786. https://doi.org/10.1016/j.celrep.2020.01.037 (2020).
4. Murayama T et al. Oncogenic Fusion Gene CD74-NRG1 Confers Cancer Stem Cell-like Properties in Lung Cancer through a IGF2 Autocrine/Paracrine Circuit. *Cancer Res*. 76(4), 974. https://doi.org/10.1158/0008-5472.CAN-15-2135 (2016).

5. Vecchi L et al. Inhibition of the AnxA1/FPR1 autocrine axis reduces MDA-MB-231 breast cancer cell growth and aggressiveness in vitro and in vivo. *Biochim Biophys Acta Mol Cell Res*. 1865(9), 1368. https://doi.org/10.1016/j.bbamcr.2018.06.010 (2018).
6. Minder P, Bayha E, Becker-Pauly C & Sterchi EE. Meprinalpha transactivates the epidermal growth factor receptor (EGFR) via ligand shedding, thereby enhancing colorectal cancer cell proliferation and migration. *J Biol Chem*. 287(42), 35201. https://doi.org/10.1074/jbc.M112.368910 (2012).
7. Wang Y et al. Interleukin-8 secretion by ovarian cancer cells increases anchorage-independent growth, proliferation, angiogenic potential, adhesion and invasion. *Cytokine*. 59(1), 145. https://doi.org/10.1016/j.cyto.2012.04.013 (2012).
8. Tang J et al. Autocrine parathyroid hormone-like hormone promotes intrahepatic cholangiocarcinoma cell proliferation via increased ERK/JNK-ATF2-cyclinD1 signaling. *J Transl Med*. 15(1), 238. https://doi.org/10.1186/s12967-017-1342-1 (2017).
9. Azoitei N et al. HSP90 supports tumor growth and angiogenesis through PRKD2 protein stabilization. *Cancer Res*. 74(23), 7125. https://doi.org/10.1158/0008-5472.CAN-14-1017 (2014).
10. Puttipanyalears C, Kitkumthorn N, Buranapraditkun S, Keelawat S & Mutirangura A. Breast cancer upregulating genes in stromal cells by LINE-1 hypermethylation and micrometastatic detection. *Epigenomics*. 8(4), 475. https://doi.org/10.2217/epi-2015-0007 (2016).
11. Trapnell C et al. Transcript assembly and quantification by RNA-Seq reveals unannotated transcripts and isoform switching during cell differentiation. *Nat Biotechnol*. 28(5), 511. https://doi.org/10.1038/nbt.1621 (2010).
12. Pertea M, Kim D, Pertea GM, Leek JT & Salzberg SL. Transcript-level expression analysis of RNA-seq experiments with HISAT, StringTie and Ballgown. *Nat Protoc*. 11(9), 1650. https://doi.org/10.1038/nprot.2016.095 (2016).
13. Melo SA et al. Cancer exosomes perform cell-independent microRNA biogenesis and promote tumorigenesis. *Cancer Cell*. 43(9), 1776. https://doi.org/10.1016/j.ccell.2025.07.022 (2025).
14. Han Z et al. RNA-seq profiling reveals PBMC RNA as a potential biomarker for hepatocellular carcinoma. *Sci Rep*. 11(1), 17797. https://doi.org/10.1038/s41598-021-96952-x (2021).
15. Zhang Y et al. Pan-cancer scRNA-seq analysis reveals immunological and diagnostic significance of the peripheral blood mononuclear cells. *Hum Mol Genet*. 33(4), 342. https://doi.org/10.1093/hmg/ddad187 (2024).
16. Zhang Y et al. Computational analysis of exosome-derived signature in TNBC: Integrating single-cell and bulk transcriptomics for prognosis prediction. *Clin Transl Sci*. 18(10), e70368. https://doi.org/10.1111/cts.70368 (2025).
17. Wu J et al. Differential gene expression in PBMCs: Insights into the mechanism how pulmonary tuberculosis increases lung cancer risk. *Gene*. 940, 149199. https://doi.org/10.1016/j.gene.2024.149199 (2025).
18. Khare D et al. Mesenchymal stromal cell-derived exosomes affect mRNA expression and function of B-lymphocytes. *Front Immunol*. 9, 3053. https://doi.org/10.3389/fimmu.2018.03053 (2018).

19. Singh S et al. RNA profile of immuno-magnetically enriched lung cancer associated exosomes isolated from clinical samples. *Cancer Genet*. 274-275, 59. https://doi.org/10.1016/j.cancergen.2023.03.008 (2023).
20. Wicherska-Pawlowska K, Wrobel T & Rybka J. Toll-like receptors (TLRs), NOD-like receptors (NLRs), and RIG-I-like receptors (RLRs) in innate immunity. TLRs, NLRs, and RLRs ligands as immunotherapeutic agents for hematopoietic diseases. *Int J Mol Sci*. 22(24). https://doi.org/10.3390/ijms222413397 (2021).
21. Hurbain J, Thommen Q, Anquez F & Pfeuty B. Quantitative modeling of pentose phosphate pathway response to oxidative stress reveals a cooperative regulatory strategy. *iScience*. 25(8), 104681. https://doi.org/10.1016/j.isci.2022.104681 (2022).
22. Gong T, Liu L, Jiang W & Zhou R. DAMP-sensing receptors in sterile inflammation and inflammatory diseases. *Nat Rev Immunol*. 20(2), 95. https://doi.org/10.1038/s41577-019-0215-7 (2020).
23. Velloso FJ, Trombetta-Lima M, Anschau V, Sogayar MC & Correa RG. NOD-like receptors: major players (and targets) in the interface between innate immunity and cancer. *Biosci Rep*. 39(4). https://doi.org/10.1042/BSR20181709 (2019).
24. Moon Y. Ribosomal alteration-derived signals for cytokine induction in mucosal and systemic inflammation: noncanonical pathways by ribosomal inactivation. *Mediators Inflamm*. 2014, 708193. https://doi.org/10.1155/2014/708193 (2014).
25. Gao Y et al. Quantitative proteomics by SWATH-MS reveals sophisticated metabolic reprogramming in hepatocellular carcinoma tissues. *Sci Rep*. 7, 45913. https://doi.org/10.1038/srep45913 (2017).
26. TeSlaa T, Ralser M, Fan J & Rabinowitz JD. The pentose phosphate pathway in health and disease. *Nat Metab*. 5(8), 1275. https://doi.org/10.1038/s42255-023-00863-2 (2023).
27. Sulic S et al. Inactivation of S6 ribosomal protein gene in T lymphocytes activates a p53-dependent checkpoint response. *Genes Dev*. 19(24), 3070. https://doi.org/10.1101/gad.359305 (2005).
28. Wang H et al. Transcriptome profiling of A549 non-small cell lung cancer cells in response to Trichinella spiralis muscle larvae excretory/secretory products. *Front Vet Sci*. 10, 1208538. https://doi.org/10.3389/fvets.2023.1208538 (2023).
29. Amin A et al. Comparative proteomics and global genome-wide expression data implicate role of ARMC8 in lung cancer. *Asian Pac J Cancer Prev*. 16(9), 3691–3696. https://doi.org/10.7314/apjcp.2015.16.9.3691 (2015).
30. Fortunato O et al. Development of a molecular blood-based immune signature classifier as biomarker for risks assessment in lung cancer screening. *Cancer Epidemiol Biomarkers Prev*. 31(11), 2020–2029. https://doi.org/10.1158/1055-9965.EPI-22-0689 (2022).
31. Chen S et al. A prospective multi-cohort study identifies and validates a 5-gene peripheral blood signature predictive of immunotherapy response in non-small cell lung cancer. *Mol Cancer*. 23(1), 247. https://doi.org/10.1186/s12943-024-02160-2 (2024).
32. Deng M, Zhang W, Yuan L, Tan J & Chen Z. HIF-1a regulates hypoxia-induced autophagy via translocation of ANKRD37 in colon cancer. *Exp Cell Res*. 395(1), 112175.

https://doi.org/10.1016/j.yexcr.2020.112175 (2020).
33. Zhang Y, Che W, Li Q & Huang W. Integrated transcriptomic and single-cell analysis reveals cell cycle dysregulation and cellular heterogeneity in lung cancer. *Discov Oncol*. 17(1), 191. https://doi.org/10.1007/s12672-025-04303-3 (2025).
34. Gyorffy B. Transcriptome-level discovery of survival-associated biomarkers and therapy targets in non-small-cell lung cancer. *Br J Pharmacol*. 181(3), 362. https://doi.org/10.1111/bph.16257 (2024).
35. Pourmir I, Gazeau B, de Saint Basile H & Fabre E. Biomarkers of resistance to immune checkpoint inhibitors in non-small-cell lung cancer: myth or reality? *Cancer Drug Resist*. 3(3), 276. https://doi.org/10.20517/cdr.2020.14 (2020).
36. Jiang Z, Zhou Y & Huang J. A combination of biomarkers predict response to immune checkpoint blockade therapy in non-Small cell lung cancer. *Front Immunol*. 12, 813331. https://doi.org/10.3389/fimmu.2021.813331 (2021).
37. Cho U, Im S & Park HS. Exploring histological predictive biomarkers for immune checkpoint inhibitor therapy response in non-small cell lung cancer. *J Pathol Transl Med*. 58(2), 49. https://doi.org/10.4132/jptm.2024.01.31 (2024).
38. Wan R et al. Discovery of tumor immune infiltration-related snoRNAs for predicting tumor immune microenvironment status and prognosis in lung adenocarcinoma. *Comput Struct Biotechnol J*. 19, 6386. https://doi.org/10.1016/j.csbj.2021.11.032 (2021).
39. Wu Q et al. Hypoxia-inducible factors: master regulators of hypoxic tumor immune escape. *J Hematol Oncol*. 15(1), 77. https://doi.org/10.1186/s13045-022-01292-6 (2022).
40. Chen Z, Han F, Du Y, Shi H & Zhou W. Hypoxic microenvironment in cancer: molecular mechanisms and therapeutic interventions. *Signal Transduct Target Ther*. 8(1), 70. https://doi.org/10.1038/s41392-023-01332-8 (2023).
41. Li J et al. FAT4 expression in peripheral blood mononuclear cells is associated with prognosis and immune cell infiltration in hepatocellular carcinoma. *Sci Rep*. 13(1), 15735. https://doi.org/10.1038/s41598-023-42560-w (2023).
42. Zuo S, Wei M, Wang S, Dong J & Wei J. Pan-cancer analysis of immune cell infiltration identifies a prognostic immune-cell characteristic score (ICCS) in lung adenocarcinoma. *Front Immunol*. 11, 1218. https://doi.org/10.3389/fimmu.2020.01218 (2020).
43. Li X et al. Comprehensive analysis of BUBs gene family in lung adenocarcinoma with immunological analysis. *Aging (Albany NY)*. 15(3), 810. https://doi.org/10.18632/aging.204517 (2023).
44. Kanahisa M & Goto S. KEGG: kyoto encyclopedia of genes and genomes. *Nucleic Acids Res*. 28(1), 27. https://doi.org/10.1093/nar/28.1.27 (2000).
45. Kanehisa M, Sato Y, Kawashiwa M, Furumichi M & Tanabe M. KEGG as a reference resource for gene and protein annotation. *Nucleic Acids Res*. 44(D1), D457. https://doi.org/10.1093/nar/gkv1070 (2016).

Tables

Table 1 is available in the Supplementary Files section.

Figures

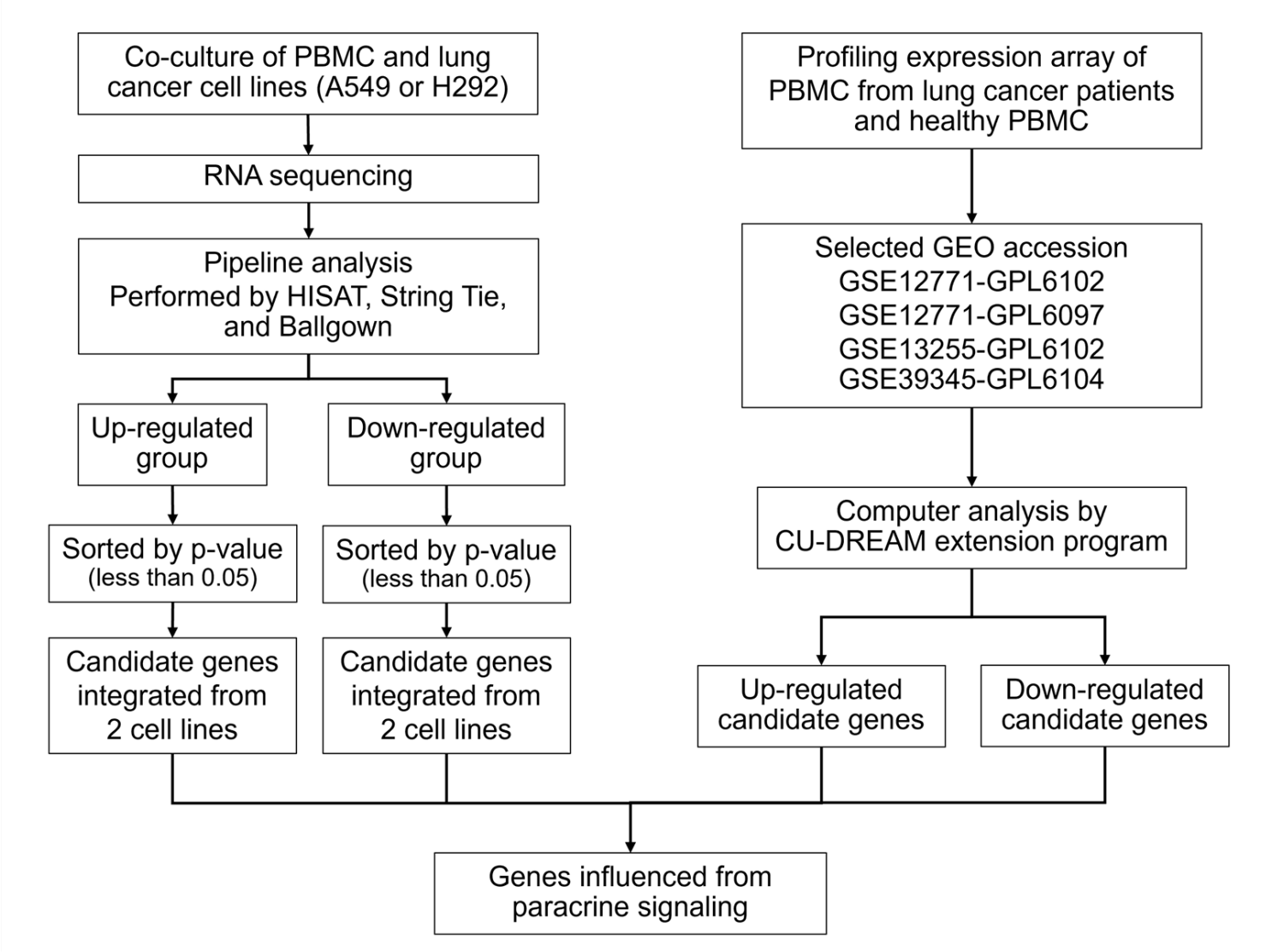


Figure 1

Study workflow for identifying candidate genes influenced by paracrine signaling. This schematic outlines the integration of two transcriptomic pipelines: an *in vitro*approach using RNA sequencing of PBMC-lung cancer cell co-cultures (left), and an *in silico* approach analyzing clinical PBMC microarray datasets from the Gene Expression Omnibus (right). Significant up- and down-regulated genes from both methods are integrated to determine the final candidate genes.

A

Cell line co-cultured with PBMC	Up-regulation			Down-regulation		
	Total Number	p value < 0.05		Total Number	p value < 0.05	
		Number	Fold change		Number	Fold change
A549	8073	170	1.08-7.46	8070	126	0.89-0.14
H292	8341	302	1.07-8.04	8342	206	0.91-0.12

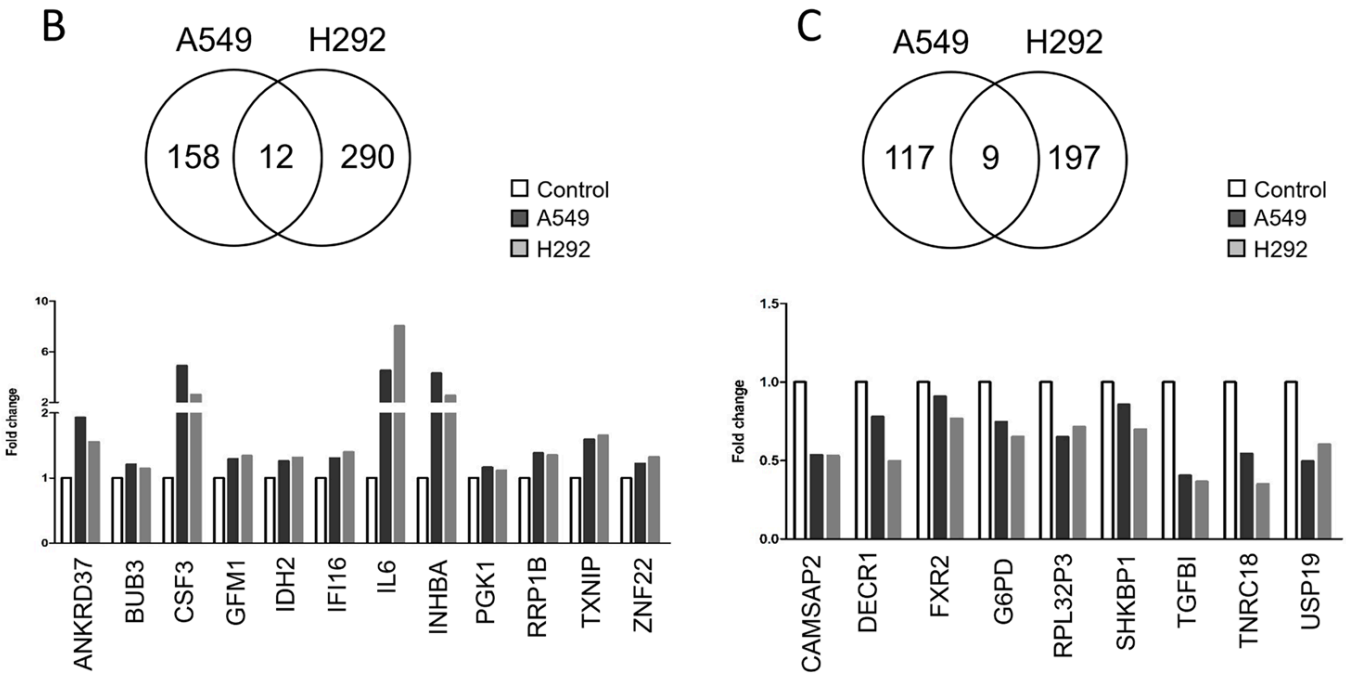


Figure 2

Unveiling the impact of paracrine signaling on gene analysis.

(A) RNA sequencing data of PBMC co-cultured with lung cancer cell lines (A549 or H292) classified by up-regulation and down-regulation, sorted by significance (p-value).

(B) Integrating RNA sequencing data of up-regulated genes from two cell lines (upper) and comparing fold change of integrated genes to control (lower).

(C) Integrating RNA sequencing data of down-regulated genes from two cell lines (upper) and comparing fold change of integrated genes to control (Lower).

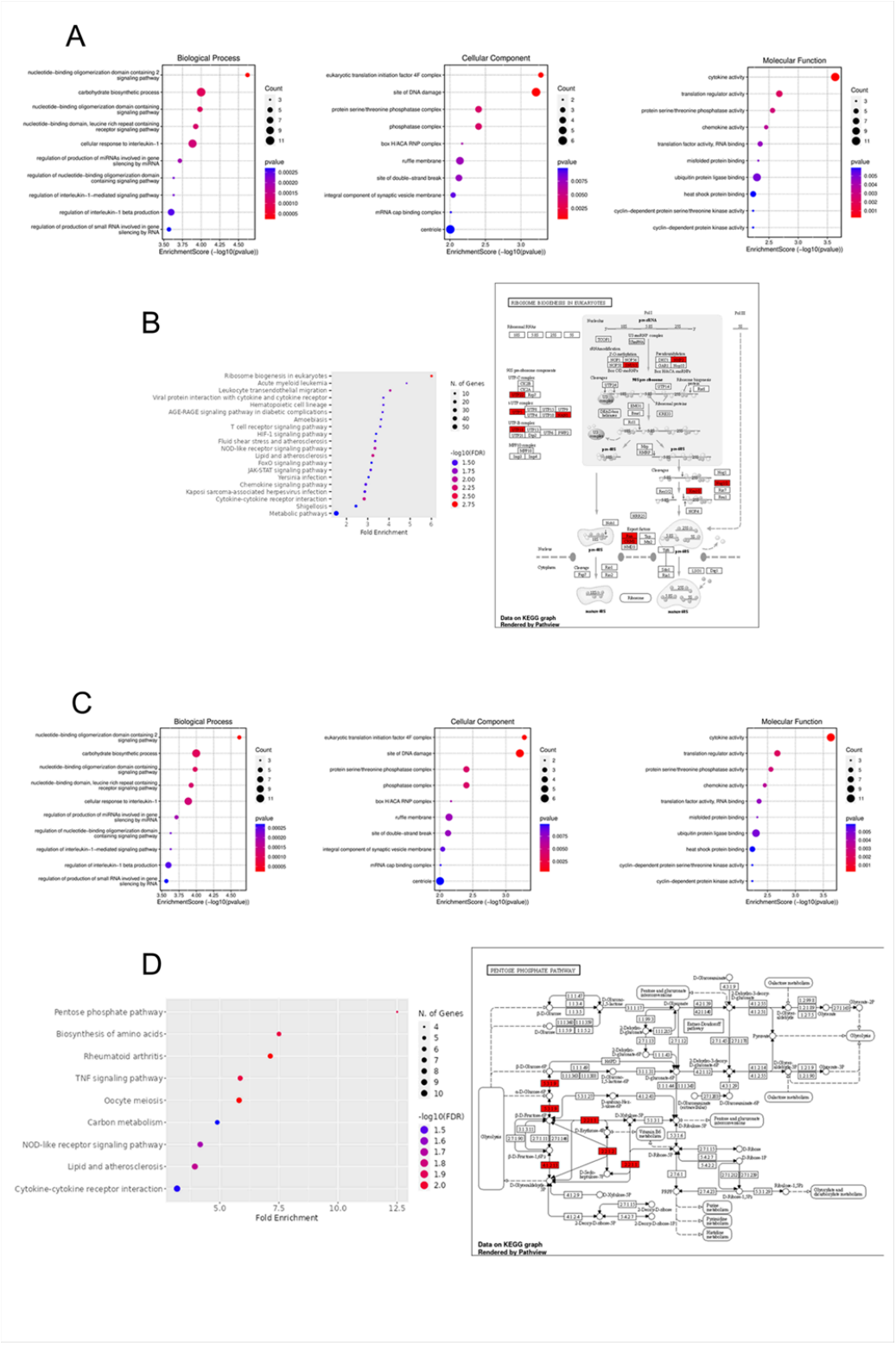


Figure 3

Gene Ontology (GO) and KEGG pathway enrichment analyses of differentially expressed genes (DEGs) from peripheral blood mononuclear cells (PBMCs) co-cultured with lung cancer cell lines. GO analysis of PBMCs co-cultured with H292 cells showed enrichment in the nucleotide-binding oligomerization domain (NOD)-containing signaling pathway, eukaryotic translation initiation factor 4F complex, and cytokine activity (A). KEGG pathway analysis revealed enrichment in the ribosome biogenesis in

eukaryotes pathway (B). Similarly, GO analysis of PBMCs co-cultured with A549 cells indicated enrichment in the same functional categories (C), while KEGG analysis demonstrated enrichment in the pentose phosphate pathway (D). Statistical enrichment was determined using the DAVID database (https://david.ncifcrf.gov/) with $P < 0.05$.

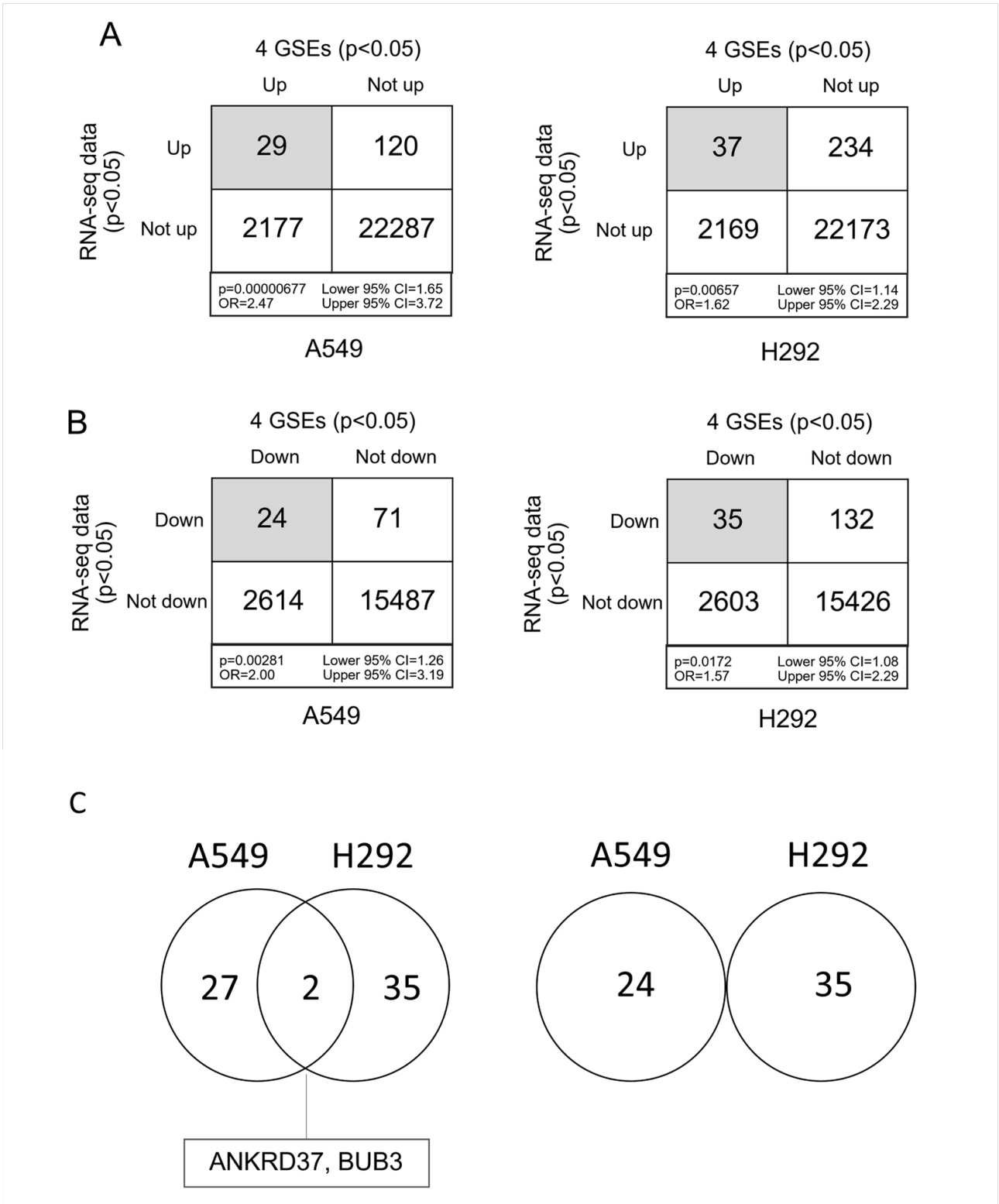


Figure 4

Integrative analysis of RNA sequencing data and expression array profiles using the CU-DREAM program in (A) Up-regulation group, (B) Down-regulation group, (C) Integration of RNA sequencing data from the up-regulation group (leaf) and down-regulation group (right) across two cell lines

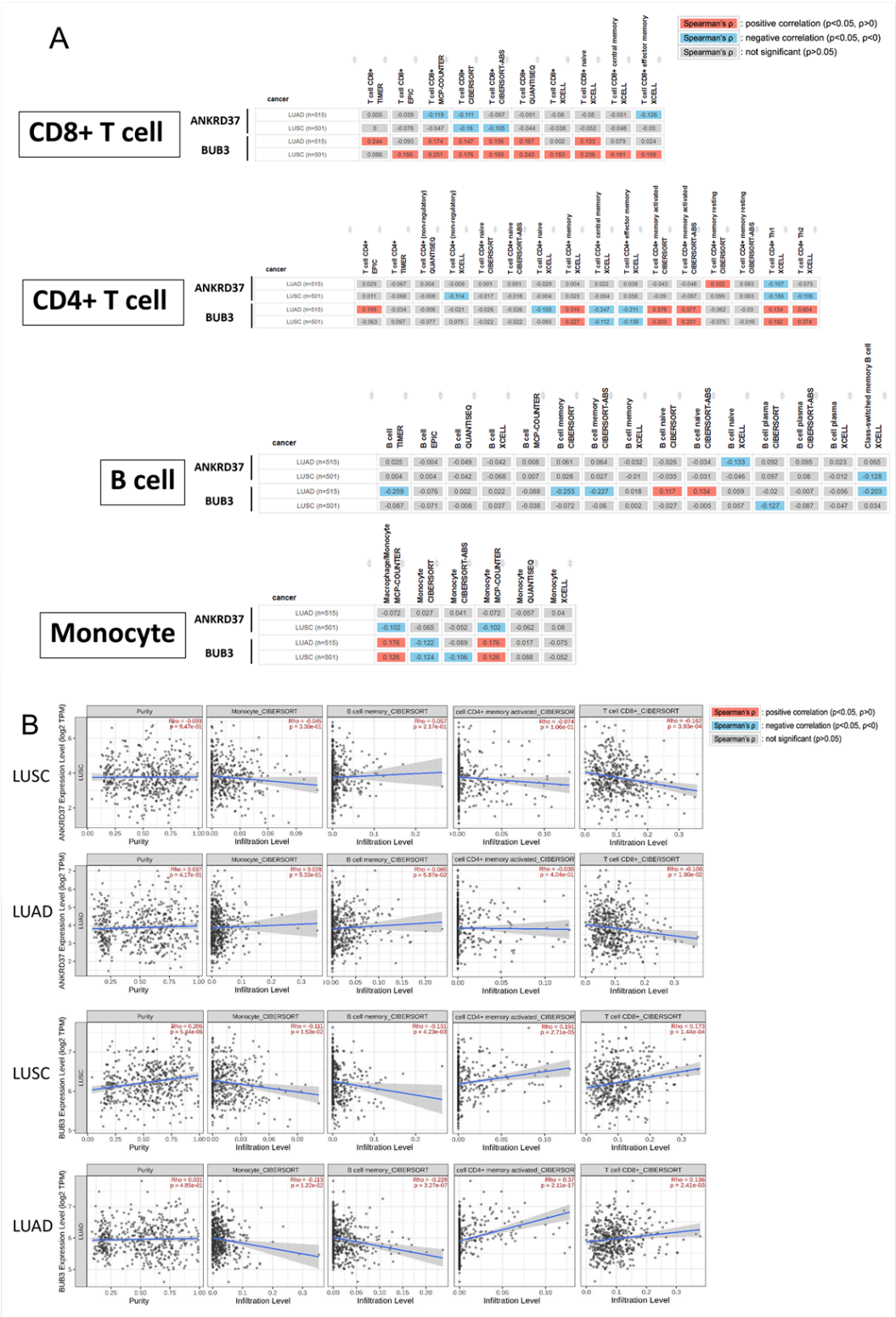


Figure 5

Visualization of immune components and gene expression correlations assessed by TIMER2.0. (A) Functional heatmaps display correlations between ANKRD37 and BUB3 expression and immune cell subpopulations, including $CD8^+$T cells, $CD4^+$T cells, B cells, and monocytes, in lung adenocarcinoma (LUAD) and lung squamous cell carcinoma (LUSC). Red boxes indicate positive correlations, while negative correlations are shown in blue. (B) Scatter plots illustrate the association ofANKRD37and BUB3expression (Log2 TPM) with purity and immune cell infiltration level in LUAD and LUSC. The blue line represents the best-fit linear regression with a 95% confidence interval.

Supplementary Files

This is a list of supplementary files associated with this preprint. Click to download.

- Table1.docx